Available online at website: https://journal.bcrec.id/index.php/bcrec

Bulletin of Chemical Reaction Engineering & Catalysis, 20 (2) 2025, 318-330

Original Research Article

Polyethyleneimine-Functionalized Magnetic Bagasse Composite for Efficient Adsorptive Removal of Yellow 4GL and Black R–S Dyes

Thi Thuy Hong Vu[1], Thi Diem Bui[1], Nguyen Le Huu Khanh[2], Thi Hong Anh Nguyen[3,*]

[1]Faculty of Chemical Engineering, Industrial University of Ho Chi Minh City, 12 Nguyen Van Bao Rd, Ho Chi Minh City 700000, Viet Nam.
[2]Tran Dai Nghia High School for the gifted, An Khanh Ward, Thu Duc, Ho Chi Minh City 700000, Viet Nam.
[3]Faculty of Chemical Engineering, Ho Chi Minh City University of Industry and Trade, 140 Le Trong Tan Street, Tay Thanh Ward, Tan Phu District, Ho Chi Minh City 700000, Viet Nam.

Received: 14th March 2025; Revised: 12th April 2025; Accepted: 13th April 2025
Available online: 16th April 2025; Published regularly: August 2025

Abstract

Efficient removal of dye contaminants from wastewater remains a significant environmental challenge. In this study, a polyethyleneimine (PEI)-modified magnetic bagasse composite was synthesized by integrating sugarcane bagasse, PEI, Fe_3O_4 nanoparticles, and glutaraldehyde as cross-linking. The synthesized material was comprehensively characterized using Scanning Electron Microscope (SEM), Brunauer-Emmett-Teller (BET) surface area, X-ray Diffraction (XRD), Thermogravimetric Analysis (TGA), and Fourier Tranform Infra Red (FTIR) techniques to elucidate its structural and physicochemical properties. Adsorption experiments were performed to investigate the effects of adsorbent dosage, initial dye concentration, pH, and contact time on the removal efficiency of Yellow 4GL and Black R-S dyes. The PEI-magnetic bagasse composite (PMBC) demonstrated impressive adsorption capacities of 185.19 mg/g for Yellow 4GL and 204.08 mg/g for Black R-S. The adsorption kinetics conformed to the pseudo-second-order model, indicating that chemisorption dominated the process, driven by electrostatic interactions and hydrogen bonding between the amino groups of PEI and the sulfonate groups of the dyes.

Keywords: Magnetic bagasse; Polyethyleneimine; Yellow 4GL; Black R-S; Wastewater treatment

How to Cite: Vu, T.T.H., Bui, T.D., Nguyen, L.H.K., Nguyen, T.H.A. (2025). Polyethyleneimine-Functionalized Magnetic Bagasse Composite for Efficient Adsorptive Removal of Yellow 4GL and Black R–S Dyes. *Bulletin of Chemical Reaction Engineering & Catalysis*, 20 (2), 318-330. (doi: 10.9767/bcrec.20368)

Permalink/DOI: https://doi.org/10.9767/bcrec.20368

1. Introduction

The growth of textile dyeing has resulted in environmental degradation, mostly from wastewater generated during the dying process. The dyes do not form complete covalent connections with textile fibers, resulting in the release of unbound pigment and hazardous byproducts into aquatic environments. Because of its chemically stable structure, textile dyes can withstand both photolytic and biodegradation processes, allowing it to survive in the environment. This persistence disturbs aquatic ecosystems by reducing light penetration, lowering dissolved oxygen levels, and endangering aquatic life. Furthermore, the slow breakdown of dyes poses health risks in locations where contaminated water is used for drinking or irrigation [1-4].

The magnetic nanoparticle and bagasse materials represent a significant advancement in the field of nanocomposites, particularly for applications in environmental remediation [5]. Magnetic nanoparticles have gained prominence due to their ability to be manipulated by external magnetic fields, enhancing their utility in

* Corresponding Author.
Email: anhnth@huit.edu.vn (T.H.A. Nguyen)

wastewater treatment. Renewable and recoverable magnetic Fe_3O_4@PEI nanoparticles were synthesized and employed for tungsten removal with a maximum adsorption capacity of 43.24 mg/g [6]. Additionally, polyethylenimine modified Fe_3O_4 nanoparticles were also applied for adsorption of protein [7], removal of Pb(II) [8] and capturing bacteria [9]. The incorporation of PEI aids in the stabilization of the nanoparticles and enhances their interaction with biological systems due to the high positive charge density of PEI, which facilitates the adsorption of negatively charged species [10]. Furthermore, the integration of bagasse as a matrix material in the magnetic nanocomposite aligns with the principles of green chemistry. Zulfiqar *et al.* highlighted the use of biochar derived from sugarcane bagasse as a support for iron oxide nanoparticles, promoting an eco-friendly synthesis approach that contrasts with traditional methods [11]. This method reduces waste and enhances the adsorption capacity of the composite for various contaminants, including dyes and pharmaceuticals. Zhao *et al.* reported that composites with PEI-modified surfaces demonstrated high adsorption capacities for various anionic dyes, indicating that similar approaches could be applied to the removal of pharmaceutical contaminants from water [10].

The removal of dyes such as Reactive Yellow 4GL, Black R-S and other textile dyes from wastewater represents a significant environmental challenge, necessitating the development of efficient adsorbents [12-14]. Recent studies have emphasized the potential of biomass-derived materials, particularly those functionalized with polyethyleneimine (PEI), for the effective adsorption of these anionic dyes. As noted by Hassan and co-workers, these materials boast high surface areas and tailored porosity, which promote dye adsorption via mechanisms including electrostatic attractions and π-π stacking interactions [15]. The study indicates that modifications to these materials can significantly enhance their dye removal capabilities, making them suitable candidates for treating dye-laden wastewater. In a more specific application, Ngamsurach *et al.* explored the modification of bagasse and bagasse fly ash with iron(III) oxide-hydroxide and zinc oxide, demonstrating their effectiveness in removing Reactive Blue 4 dye from aqueous solutions. Their findings revealed that the modified materials achieved over 90% dye removal efficiency, with a maximum adsorption capacity of 10.277 mg/g [16]. Birniwa *et al.* demonstrated that a polypyrrole-PEI nano-adsorbent effectively removed methylene blue from aqueous solutions, indicating that similar approaches could be applied to Yellow 4GL and Black R-S [17].

This study underscores the potential modification of agricultural waste products (sugarcane bagasse) with PEI as effective adsorbents for Yellow 4GL and Black R-S dyes removal. The separation of adsorbents was improved by using magnetic nanoparticles. The incorporation of PEI into adsorbent materials has been shown to significantly improve the adsorption performance. This modification allows for increased interaction between the adsorbent and the dye molecules, thereby improving removal efficiencies. The structure of as-prepared materials were characterized SEM, BET, XRD, TGA, and FTIR techniques. The effects of adsorbent dosage, initial dye concentration, pH, and contact time to the removal efficiency of Yellow 4GL and Black R-S dyes on polyethyleneimine-modified magnetic bagasse composite.

2. Materials and Method

2.1 Materials

Iron(II) sulfate ($FeSO_4.7H_2O$), iron(III) chloride ($FeCl_3.6H_2O$), glutaraldehyde and polyethyleneimine were purchased from Sigma-Aldrich. Additionally, ethanol, hydrochloric acid, and sodium hydroxide were acquired from Xilong Scientific Co., Ltd. (China). All chemical reagents were utilized as obtained, without further purification.

2.2 Preparation of Magnetic Bagasse and PEI-magnetic Bagasse

The sugarcane bagasse was collected from Go Vap market (Ho Chi Minh City, Viet Nam) and washed three times with water to remove excess sugar and impurities. The cleaned sugarcane bagasse is then dried at 60–70 °C and ground using a disc mill to obtain particles sized 0.5–1 mm. To synthesize magnetic bagasse, a bagasse/Fe_3O_4 ratio of 8/2 is used [18]. $FeCl_3.6H_2O$ and $FeSO_4.7H_2O$ (Ratio of Fe2+: Fe^{3+} = 1:2) are dissolved in 150 mL of distilled water, followed by the addition of 2 g of bagasse. After stirring, NaOH solution is slowly added until the pH reaches 11–12. The mixture is then placed in an autoclave and heated at 80 °C for 6 hours. After cooling, the product is filtered, washed, and dried at 60–70 °C until a constant mass is achieved, yielding magnetic bagasse [19-20].

The PEI-modified magnetic bagasse composite (PMBC) was prepared by adding 1 g of magnetic bagasse into 100 mL of a polyethyleneimine solution at concentrations of 10%. The bagasse-PEI mixture was then refluxed at 65 °C for 6 h, after which a 1% (w/v) glutaraldehyde solution was added to facilitate cross-linking. Finally, the product was filtered, washed with deionized water, and dried at 70-80

°C until a constant weight was achieved, yielding the modified bagasse material.

2.3 Structural Analysis

The structural analysis of PEI-modified bagasse composite were characterized using techniques include scanning electron microscopy (SEM), Fourier-transform infrared spectroscopy (FT-IR), X-ray diffraction (XRD), thermogravimetric analysis (TGA), and Brunauer-Emmett-Teller (BET) surface area analysis. Scanning Electron Microscopy (SEM) is utilized to investigate the surface morphology and characteristics of modified bagasse. The SEM images of prepared materials were measured using field emission scanning electron microscope (JSM-S4800, Tokyo, Japan). The FT-IR spectra recorded in the range of 4500 to 500 cm^{-1} with a Bruker Tensor 27 spectrometer (Germany). The XRD patterns obtained in the 2θ range of 10 to 80° on a LabX XRD-6100, Shimadzu, Japan. Thermogravimetric analysis (TGA) is performed on TGA55 (TA Instruments) under nitrogen at a flow rate of 50 mL/min and the ramping the temperature at 10 °C/min from 30 to 825 °C. Brunauer-Emmett-Teller (BET) analysis is measured at 77 K using a TriStar II 3020-Micromeritics gas adsorption analyzer. The magnetic characteristics were evaluated using a Lake Shore 7404 vibrating sample magnetometer under a magnetic field sweep from -15 kOe to 15 kOe at room temperature. The concentration of dyes were measured by the Cary 3500 UV-Vis spectrophotometer in the range of 400–600 nm.

2.4 Adsorption of Yellow 4GL and Black R – S on PEI-magnetic Bagasse

The effect of adsorbent dose was conducted at 0.01, 0.02, and 0.03 g PMBC, the material was added to 50 mL (50 mg/L) dye solutions (Yellow 4GL or Black R–S) under stirring at 200 rpm for 150 min. The influence of dye concentration and initial time were performed using 0.03 g of adsorbent and 50 mL of different Yellow 4GL or Black R–S dye solutions ranging from of 25, 50, 75, 100, 125, and 150 mg/L. The effect of pH was carried at values of 2, 4, 6, 8, and 10. The concentration of dyes were measured by the Cary 3500 UV-Vis spectrophotometer at 428 nm for Yellow 4GL and Black R–S at 555 nm. The removal efficiency was calculated as Equation (1):

$$\%\, Removal = \frac{C_0 - C_t}{C_0} \times 100\% \quad (1)$$

where, C_0 (mg/L) and C_t (mg/L) are the concentration of dyes at the initial at time t, respectively,

2.5 Kinetic Study

The adsorption kinetics were investigated by monitoring the change in the dyes concentration. A 0.03 g portion of the PMBC was introduced into 50 mL of a 50 mg/mL each dye solution, and the mixture was continuously stirred at 200 rpm under isothermal conditions. At predetermined intervals (5, 10, 20, 30, 60, 90, 120, and 150 min), aliquot was withdrawn and analyzed using UV-Vis spectrophotometry at the characteristic wavelength. The resulting kinetic data were subsequently interpreted using relevant kinetic models:
First-order kinetic model:

$$ln(q_e - q_t) = \ln q_e - K_1 t \quad (2)$$

Second-order kinetic model:

$$\frac{t}{q_t} = \frac{1}{K_2 q_e^2} + \frac{t}{q_e} \quad (3)$$

where, q_t and q_e represent the amounts of dye adsorbed at time t and at equilibrium, respectively, and K_1 and K_2 are the rate constants for the first-order and second-order kinetic models. The kinetic constants are determined from the linear regression plots: ln (q_e–q_t) versus for the first-order model, and versus for the second-order model. The best-fitting model is selected based on the correlation coefficient (R^2).

2.6 Adsorption Isotherm Models

Adsorption isotherm models were employed to interpret equilibrium data and assess the mechanism and characteristics of the adsorption process. PMBC were introduced into solutions with initial concentrations of 25, 50, 75, 100, 125, and 150 mg/mL, and the mixtures were stirred at 200 rpm under constant temperature until equilibrium was reached. The residual dyes concentration were measured using UV-Vis spectrophotometry to determine the adsorbed amount (q_e) and the equilibrium concentration (C_e).

The data were then analyzed using the Langmuir (monolayer adsorption, K_L, q_m), Freundlich (heterogeneous adsorption, K_F, n), Dubinin-Radushkevich (adsorption energy, β), where the model parameters were obtained via linear regression, and the best-fit model was selected based on the correlation coefficient (R^2):

Langmuir Equation:

$$\frac{1}{q_e} = \frac{1}{q_m K_L} \times \frac{1}{C_e} + \frac{1}{q_m} \quad (4)$$

in which, q_m (mg/g) is the maximum adsorption capacity, and K_L (L/mg) is the Langmuir constant.

Freundlich Equation:

$$ln\ q_e = \ln K_F + \frac{1}{n} \ln C_e \quad (5)$$

in which, K_F (mg/g)(L/mg)1/n is the Freundlich constant, and n is the index characterizing heterogeneity.

Dubinin-Radushkevich Equation:

$$ln\ q_e = ln\ q_m - \beta\ .\varepsilon^2 \quad (6)$$

in which, $\varepsilon = RT \ln(1+1/C_e)$ is the Polanyi potential (kJ.mol^{-1}), β (mol^2/kJ^2) is the constant related to free energy, and q_m is the maximum adsorption capacity.

2.7 Thermodynamic Study

The adsorption experiments were conducted at various temperatures (298, 308, and 318 K) with a fixed initial dye concentration of 50 mg/mL. Once equilibrium was reached, the remaining dye concentration in the solution was measured using UV-Vis spectroscopy. From these data, equilibrium parameters such as the amount of dye adsorbed on the PMBC surface (q_e) and the equilibrium constant (K_c) were calculated. Additionally, thermodynamic parameters, including Gibbs free energy (ΔG°), enthalpy (ΔH°), and entropy (ΔS°), were determined using the following equations:

$$ln\ q_e = ln\ q_m - \beta\ .\varepsilon^2 \quad (7)$$

$$\ln K_c = \frac{\Delta S^o}{R} - \frac{\Delta H^o}{RT} \quad (8)$$

in which, R is the ideal gas constant and T is the temperature (K). A plot of ln K_c versus 1/T is used to determine ΔH^o and ΔS^o.

3. Results and Discussion

3.1 Characterization of Material

The bagasse from sugarcane was cleaned by washing with distilled water to remove impurities, resulting in a white species. After drying, the bagasse was sieved to a size range of 0.5–1 mm. Fe_3O_4 nanoparticles were incorporated onto the surface of the bagasse through a precipitation reaction, forming magnetic bagasse. Polyethyleneimine (PEI) was then applied to the surface of the magnetic bagasse using glutaraldehyde as a cross-linking agent, producing a PEI-magnetic bagasse composite (PMBC). SEM analysis showed that the PEI-

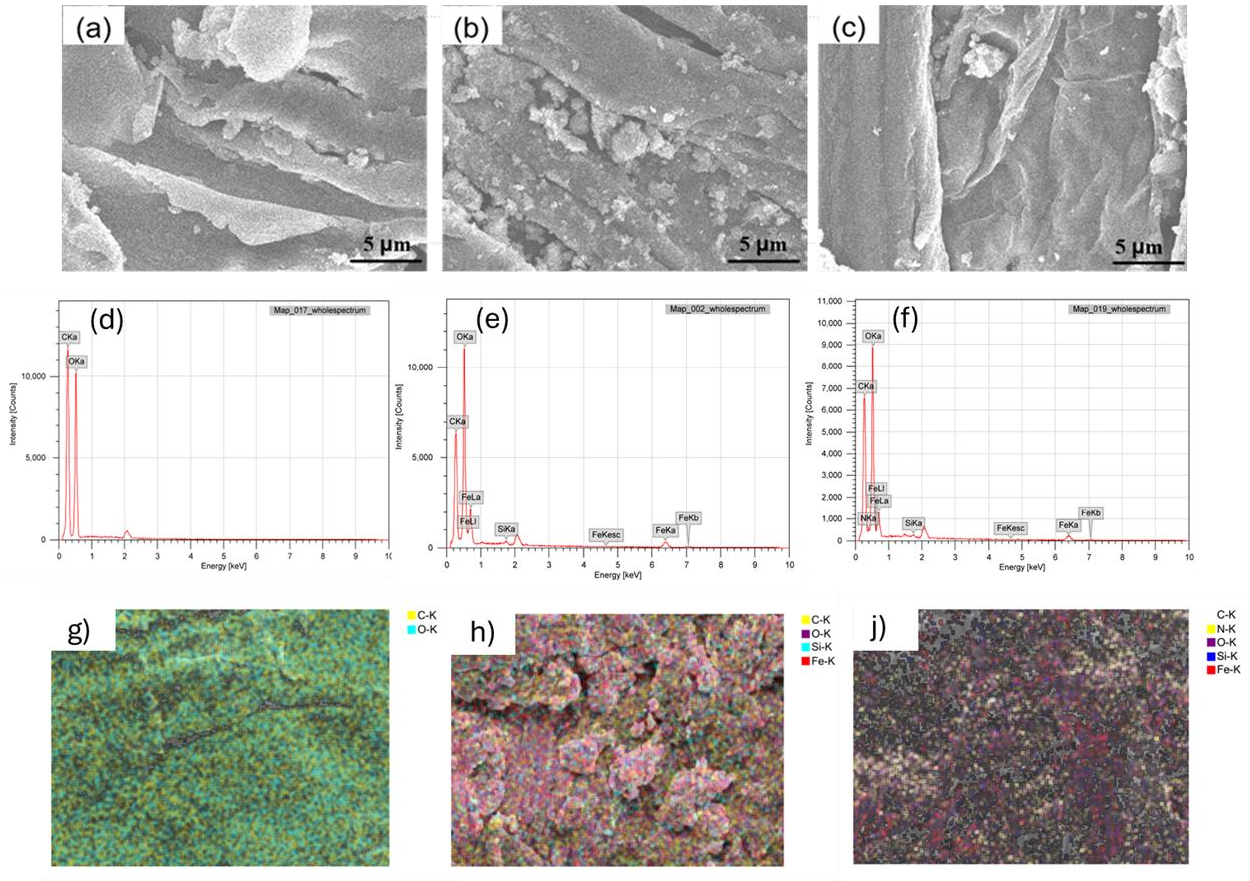

Figure 1. SEM images of (a) raw bagasse, (b) magnetic bagasse, (c) PEI-magnetic bagasse composite; EDS of (d) raw bagasse, (e) magnetic bagasse, (f) PEI-magnetic bagasse composite and EDX mapping analysis of (g) raw bagasse, (h) magnetic bagasse, (j) PEI-magnetic bagasse composite.

coated magnetic bagasse maintained a porous, interwoven structure with network-like pores and uneven distribution of Fe_3O_4 nanoparticles. The micrometer-sized pores, intrinsic to the cellulose structure of the bagasse, were preserved after chemical activation. The modification process partially removed hemicellulose and lignin, exposing the cellulose fiber network and generating additional pores, thereby increasing the surface area (Figures 1 a-c). The uneven distribution of Fe_3O_4 nanoparticles on the surface was likely due to non-uniform mixing or precipitation conditions during the composite synthesis. The final PEI modification introduced functional amino groups, further enhancing the material's adsorption performance while preserving its porous nature. These structural features contribute to a high adsorption capacity and magnetic properties, allowing for the material's reusability. The EDS analysis revealed that raw bagasse contains approximately 58% carbon (C) and 42% oxygen (O). In the case of magnetic bagasse, the composition included 46.94% C, 43.13% O, and 9.93% iron (Fe), confirming the incorporation of Fe_3O_4 nanoparticles. For the PEI-functionalized magnetic bagasse, EDS results showed 51.48% C, 41.00% O, 7.25% Fe, and the presence of 0.27% nitrogen (N), indicating successful PEI modification (Figures 1 d-j).

The TGA investigation of PEI-magnetic bagasse reveals its thermal stability and decomposition behavior from 30 to 800 °C. Moisture evaporation on the composite surface causes initial weight loss (6.935% below 200 °C), but substantial decomposition (44.271% between 200 and 400 °C) results from the breakdown of organic components such as cellulose, lignin, and PEI. Further degradation (3.767% between 400-600 °C) suggests residual organic matter loss, while 11.957% weight loss between 600-800 °C is attributable to oxidative breakdown and carbonization of any remaining organic residues. The remaining 30% mass indicates the presence of magnetic and inorganic leftovers (Figure 2a) [21]. Compared to raw bagasse, which typically leaves a final residue of 18%, and magnetic bagasse with 25%, the higher thermal stability of PEI–magnetic bagasse further supports effective material modification [22,23].

BET analysis determined a specific surface area of 30.051 m^2/g, a pore volume of 0.069 cm^3/g, and an average pore diameter of 3.4905 nm, confirming the mesoporous nature of the material, which is favorable for adsorption applications (Figure 2b). In comparison, raw bagasse exhibits a surface area of only 4.6 m^2/g and pore volume of 0.007 cm^3/g [24], while Fe_3O_4-modified bagasse (without PEI) shows a larger surface area of 66.54 m^2/g but smaller average pore diameter of 1.6 nm.

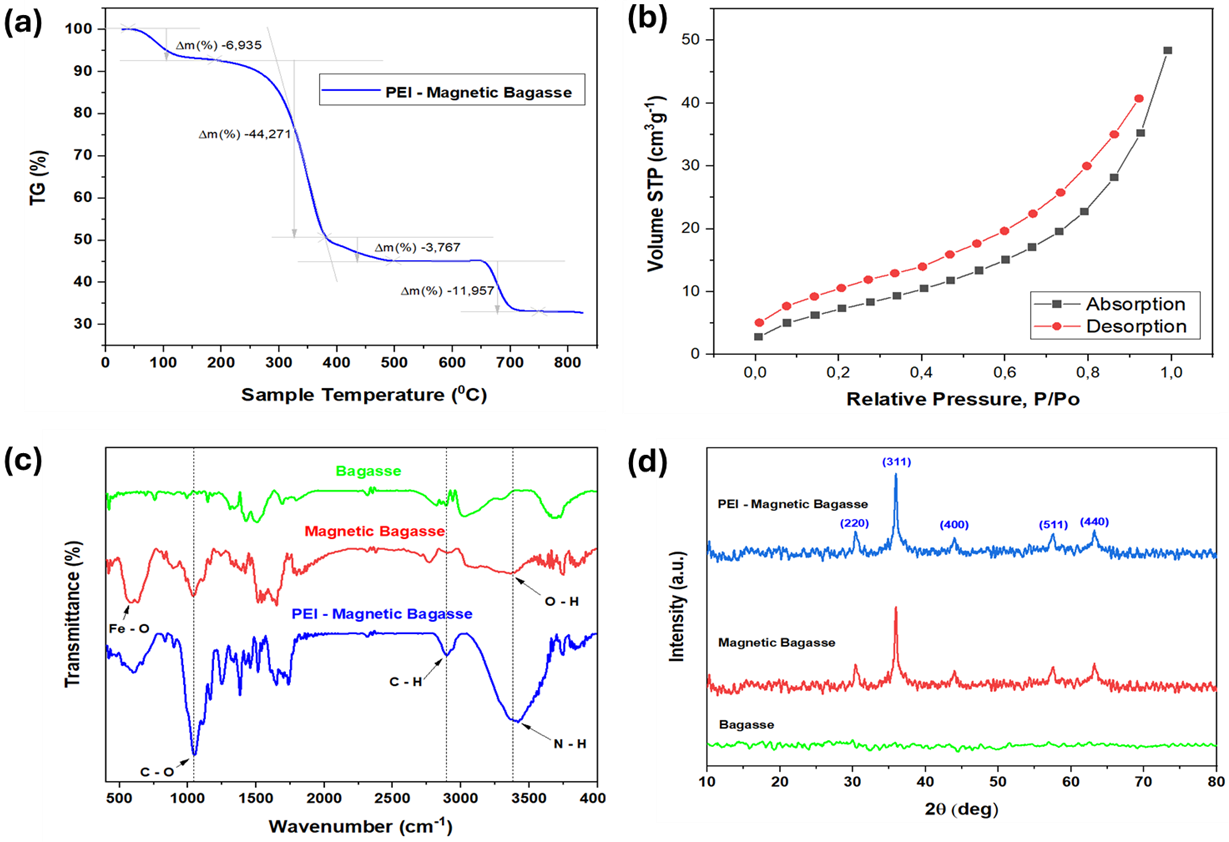

Figure 2. (a) TGA curve, (b) BET analysis, (c) FT-IR spectrum, and (d) XRD pattern of as prepared materials.

These differences highlight that PEI coating increases pore diameter and slightly reduces surface area due to partial pore blockage, but overall maintains favorable mesoporosity for adsorption.

The FTIR spectra of bagasse, magnetic bagasse, and PEI-magnetic bagasse are presented in Figure 2c. The raw bagasse spectrum (green line) exhibits a broad peak around 3300–3400 cm^{-1} corresponds to O–H stretching vibrations, which are indicative of hydroxyl groups commonly found in cellulose and hemicellulose. A peak near 2900 cm^{-1} is attributed to C–H stretching vibrations of aliphatic chains. Additionally, strong absorption in the region of 1000–1700 cm^{-1} corresponds to various functional groups such as carbonyl (C=O), aromatic skeletal vibrations from lignin (C=C), and ether linkages (C–O–C). In the case of magnetic bagasse (red line), the intensity of the O–H and C–H peaks slightly decreases, likely due to their interaction with magnetic nanoparticles. A new peak appearing around 580–600 cm^{-1} is associated with Fe–O stretching vibrations, which confirm the incorporation of Fe_3O_4 into the bagasse matrix. The PEI-magnetic bagasse spectrum (blue line) demonstrates additional bands around 3300–3500 cm^{-1} suggest the presence of N–H stretching vibrations from primary and secondary amine groups in PEI. Bands appearing near 1600–1650 cm^{-1} are likely due to N–H bending and C–N stretching vibrations of PEI.

XRD analysis further confirmed the crystalline structure of Fe_3O_4, exhibiting characteristic peaks at $2\theta \approx 30.1°$, 35.5°, 43.2°, 53.6°, 57.2°, and 62.8°, while the broad peak at $2\theta \approx 15°–25°$ reflects the amorphous nature of cellulose (Figure 2d). A slight reduction in Fe_3O_4 peak intensity indicates the successful coating of PEI onto the magnetic bagasse surface.

Figure 3 compares the magnetization curves of virgin Fe_3O_4 and the PEI-magnetic bagasse composite under a magnetic field ranging from -15 kOe to +15 kOe at room temperature. Pure Fe_3O_4 has strong saturation magnetization (68.86 emu/g), coercivity (44.34 Oe), and remanent magnetization (4.39 emu/g), indicating ferrimagnetic nanoparticles. In comparison, the PEI-magnetic bagasse composite has a lower saturation magnetization (5.98 emu/g), remanent magnetization (0.17 emu/g), and coercivity (11.18 Oe), which is mostly owing to the non-magnetic bagasse and polymeric PEI components. Despite the decrease in magnetic parameters, the composite remains easily separable by a simple magnet, illustrating that the Fe_3O_4 incorporation effectively retains sufficient magnetic functionality while improving handling and reusability in aqueous systems.

3.2 Adsorption Performance of PEI-magnetic Bagasse

3.2.1 Effect of various materials

Figure 4 illustrates the dye removal efficiencies of three different adsorbents—bagasse, magnetic bagasse, and PEI-magnetic bagasse—for two anionic dyes, Black R-S and

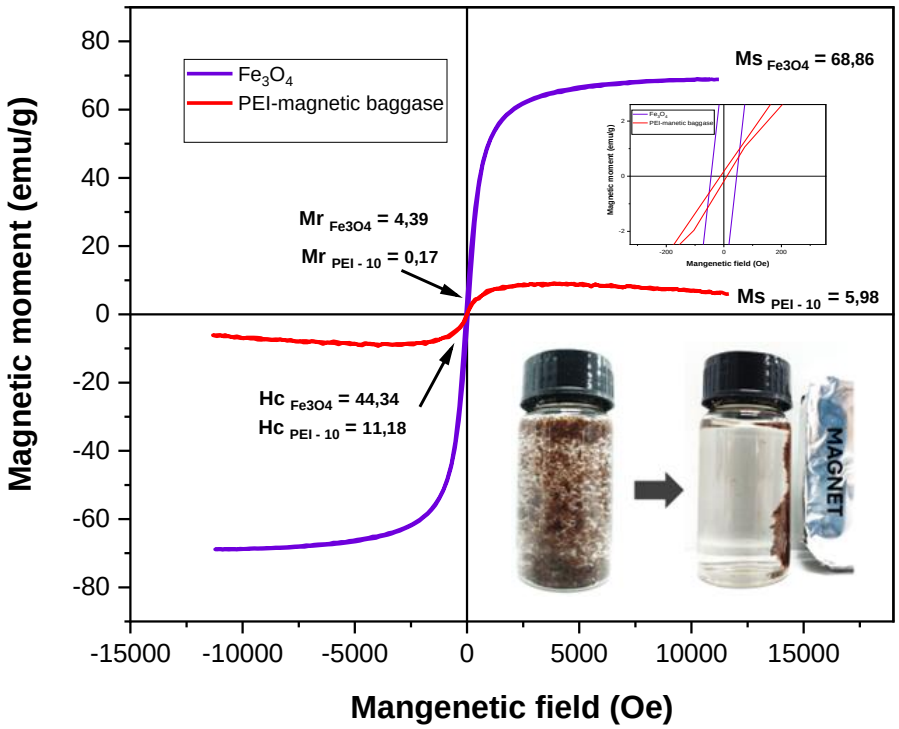

Figure 3. M-H curves of PEI-magnetic bagasse (Right up inset: hysteresis loops in expanded scale. Right down inset: the photographs of applying an external magnetic field on PMBC and its suspension in water.

Yellow 4GL. The raw bagasse shows moderate adsorption efficiencies of 46.45% and 38.43% for Black R-S and Yellow 4GL, respectively. Incorporating Fe_3O_4 nanoparticles into bagasse to create magnetic bagasse enhances the adsorption capacity to 66.84% for Black R-S and 54.25% for Yellow 4GL. The significant improvement is observed with the PEI-magnetic bagasse composite, which achieves removal efficiencies of 96.89% for Black R-S and 94.64% for Yellow 4GL. This marked enhancement is primarily due to the strong electrostatic interactions between the positively charged amine groups on polyethyleneimine and the negatively charged sulfonate groups on the dye molecules. Additionally, the PEI coating introduces extra binding sites, further promoting dye uptake. Thus, the combination of bagasse's inherent adsorptive properties, the magnetic separability imparted by Fe_3O_4, and the functionalization with PEI results in a highly effective and easily recoverable adsorbent for textile dye removal.

3.2.2 Effect of material mass

Figure 5 demonstrates the influence of adsorbent dosage on the removal efficiencies of Black R-S and Yellow 4GL dyes. As the mass of the adsorbent increases from 0.01 g to 0.03 g, the removal percentages for both dyes rise substantially. At the lowest dosage (0.01 g), Black R-S and Yellow 4GL show removal efficiencies of 85.2% and 83.6%, respectively. When the dosage is increased to 0.02 g, removal rates improve to 90.3% for Black R-S and 89.8% for Yellow 4GL. The highest dosage (0.03 g) yields the most effective dye removal, reaching 96.1% for Black R-S and 94.2% for Yellow 4GL. When the dosage increased over 0.03 g, the removal efficiency has not increased. This can be attributed to the greater availability of active adsorption sites and surface area at higher dosages, which enhances dye uptake. The similarity in removal efficiencies for dyes were also reported previously.

3.2.3 Effect of pH on Yellow 4GL and Black R – S removal

Figure 6a demonstrates how solution pH influences the removal efficiency of Black R-S and Yellow 4GL dyes. Under strongly acidic conditions (pH 2), both dyes exhibit relatively lower removal efficiencies, about 85% for Black R-S and 82% for Yellow 4GL. As the pH rises to near-neutral levels (6–7), removal efficiencies peak at around 96% for Black R-S and 95% for Yellow 4GL. At alkaline conditions (pH of 10), the removal efficiency decreases slightly, likely due to hydroxide ions (OH^-) competing for adsorption sites. In acidic media, although PEI becomes more positively charged which theoretically favors the adsorption of anionic dyes excess H^+ ions can compete with dye anions for available adsorption sites. This competitive adsorption effect significantly reduces the dye uptake. Furthermore, high protonation levels may lead to electrostatic repulsion among $-NH_3^+$ groups, slightly altering the structure of the adsorbent and hindering access to internal binding sites.

The point of zero charge (pHpzc) of PMBC is 6.3, so when the pH is below this value, the adsorbent surface becomes positively charged, thereby enhancing electrostatic attraction with the negatively charged dye molecules (Figure 6b). At higher pH levels, the surface charge is predominantly negative, reducing electrostatic interactions and increasing competition from OH^-. Consequently, near-neutral pH conditions offer the most favorable environment for dye adsorption, underscoring the effectiveness of the adsorbent in typical wastewater treatment scenarios.

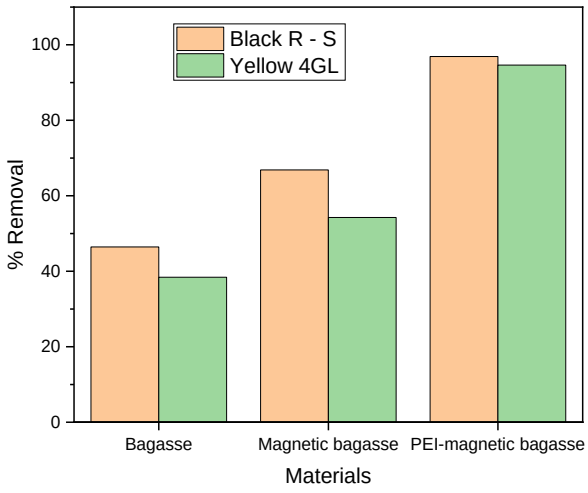

Figure 4. Effect of various materials on the adsorption of Black R-S and Yellow 4GL (0.03 g, material, 50 mL of Yellow 4GL or Black R–S dye, concentration 50 mg/mL).

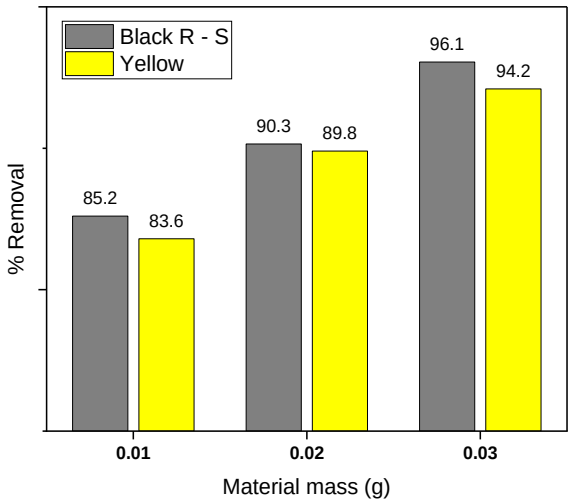

Figure 5. Effect of material mass on the adsorption of Black R-S and Yellow 4GL (50 mL of Yellow 4GL or Black R–S dye, concentration 50 mg/mL).

3.2.4 Effect of initial time and concentration on Yellow 4GL and Black R – S removal

Figures 7 depict the removal efficiency of Yellow 4GL and Black R-S at different initial dye concentrations (25–150 mg/L) onto PMBC. In both cases, the removal percentage rapidly increases at lower concentrations and plateaus at higher concentration. For instance, at an initial concentration of 25 mg/L, the complete removal (about 100% for Yellow 4GL and Black R-S) is observed within 20 min, indicating that sufficient active sites are readily available on the adsorbent surface. As the initial concentration increases to 150 mg/L, the removal efficiencies decrease to about 71.4 and 74.8% for Yellow 4GL and Black R-S, respectively. This can explain due to a greater number of dye molecules competing for a finite number of adsorption sites. The similar result was previously reported [25,26].

3.2.5 Effect of temperature on Yellow 4GL and Black R–S removal

Figure 8 depicts the influence of temperature on the removal efficiency of Yellow 4GL and Black R-S over time. In both cases, increasing the temperature from 20 °C to 60 °C leads to an enhanced dye removal rate and a higher equilibrium removal percentage, indicating that the adsorption process is likely endothermic. At higher temperatures, dye molecules possess greater kinetic energy, which facilitates their diffusion to the adsorbent surface and promotes stronger interactions with available adsorption sites. For Yellow 4GL, the removal efficiencies increased to around 90–95% within 20–30 min with temperature from 20 to 60 °C, with only a slight improvement observed at higher temperatures. In contrast, Black R-S demonstrates a more pronounced temperature dependence, achieving notably higher removal efficiencies at 50 °C and 60 °C (about 94.3%)

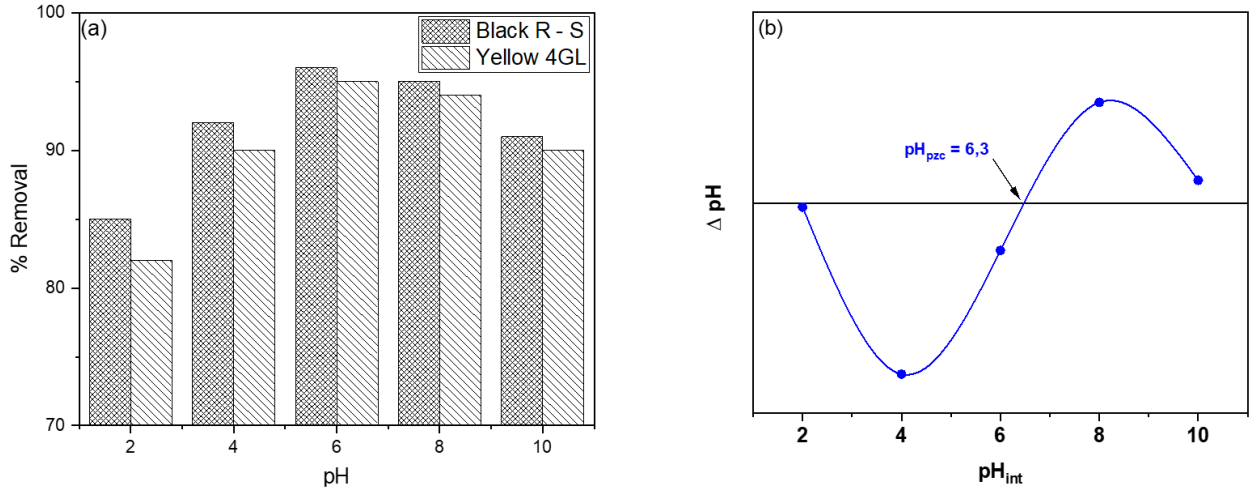

Figure 6. (a) Effect of pH on the Yellow 4GL and Black R-S removal and (b) pH_pzc of PMBC (0.03 g material, 50 mL of Yellow 4GL or Black R–S dye, concentration 50 mg/mL).

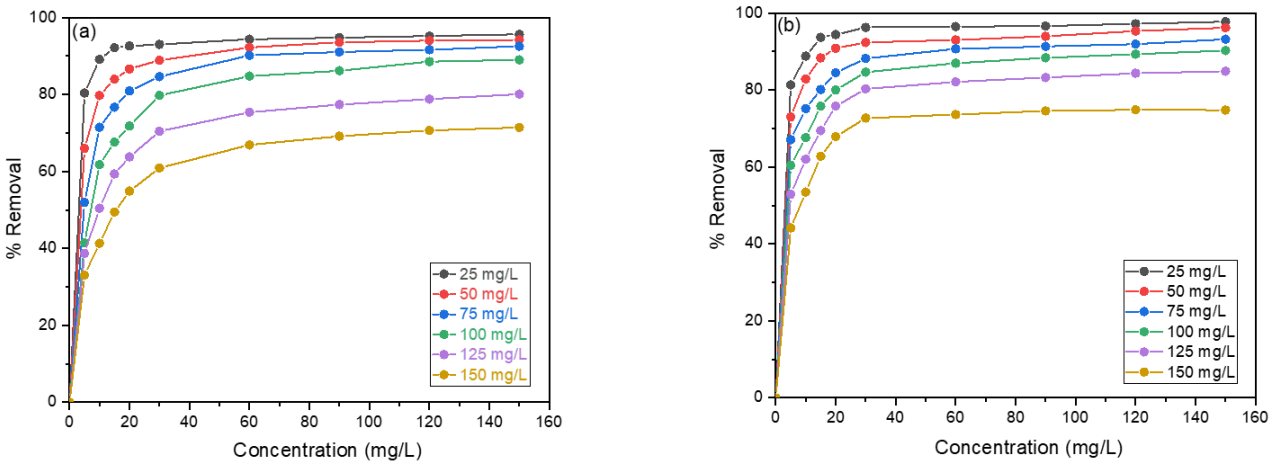

Figure 7. (a) Effect of Yellow 4GL and (b) Black R-S concentration on removal efficiency (0.03 g material, 50 mL of Yellow 4GL or Black R–S dye).

compared to 20 °C or 30 °C (84.7%). This difference suggests that Black R-S may have a higher activation energy for adsorption or that its molecular structure interacts more favorably with the adsorbent at elevated temperatures [18,27,28].

3.3 Isothermal Adsorption Study

The data show that the Langmuir model provides the best fit for the adsorption of both Yellow 4GL and Black R-S, as evidenced by its highest R^2 values (0.996 for Yellow 4GL and 0.998 for Black R-S). This suggests adsorption on a uniform, homogeneous surface. Notably, Black R-S exhibits a greater maximum adsorption capacity (qm = 204.08 mg/g) compared to Yellow 4GL (qm = 185.19 mg/g), indicating that the adsorbent has a stronger affinity for Black R-S. The Temkin model also achieves relatively high R^2 values (0.942 for Yellow 4GL and 0.987 for Black R-S), highlighting the significant influence of adsorbent–adsorbate interactions. In contrast, the Dubinin–Radushkevich (D–R) model shows lower R^2 values (0.730 and 0.840), indicating that the adsorption process does not follow a heterogeneous mechanism (Table 1) [25].

3.4 The Kinetic Study of Adsorption

The pseudo-first order and pseudo-second order parameters for the adsorption of Yellow 4GL and Black R-S dyes at various initial concentrations (25–150 mg/L) are presented in Table 2. Across all concentrations, the pseudo-second order model describes the adsorption process more accurately than the pseudo-first order model with correlation coefficients (R^2 ~ 1.0000). Furthermore, the equilibrium adsorption capacities (q_e) predicted by the pseudo-second order model are significantly higher than those estimated by the pseudo-first order model, suggesting that chemisorption dominates the dye-adsorbent interaction. For Yellow 4GL, the maximum q_e by the pseudo-second order model increases from 62.50 mg/g (C_0 = 25 mg/L) to 263.16 mg/g (C_0 = 125 mg/L). A similar trend is observed for Black R-S, where q_e rises from 60.98 mg/g (C_0 = 25 mg/L) to 270.27 mg/g (C_0 = 125 mg/L). Additionally, the rate constants (k_2 and k_1) decreased with increasing initial dye concentration, likely reflecting mass transfer limitations and competition for active sites at higher concentrations.

Figure 9 illustrates the intra-particle diffusion plots (q_t vs. $t^{1/2}$) for the adsorption

Table 1. Isotherm parameters for the adsorption of Yellow 4GL and Black R-S onto PMBC.

Dye	Langmuir			Freundlich		
	q_m	K_L	R^2	K_F	n	R^2
Yellow 4 GL	185.185	0.505	0.996	76.47	4.068	0.981
Black R-S	204.082	0.333	0.998	58.036	2.716	0.958

Dye	Rubinin-Radushkevich			Tempkin		
	q_m	β	R^2	A_T	b_T	R^2
Yellow 4 GL	134.976	0.0010	0.730	86.491	0.041	0.942
Black R-S	181.218	0.0031	0.840	59.502	0.027	0.987

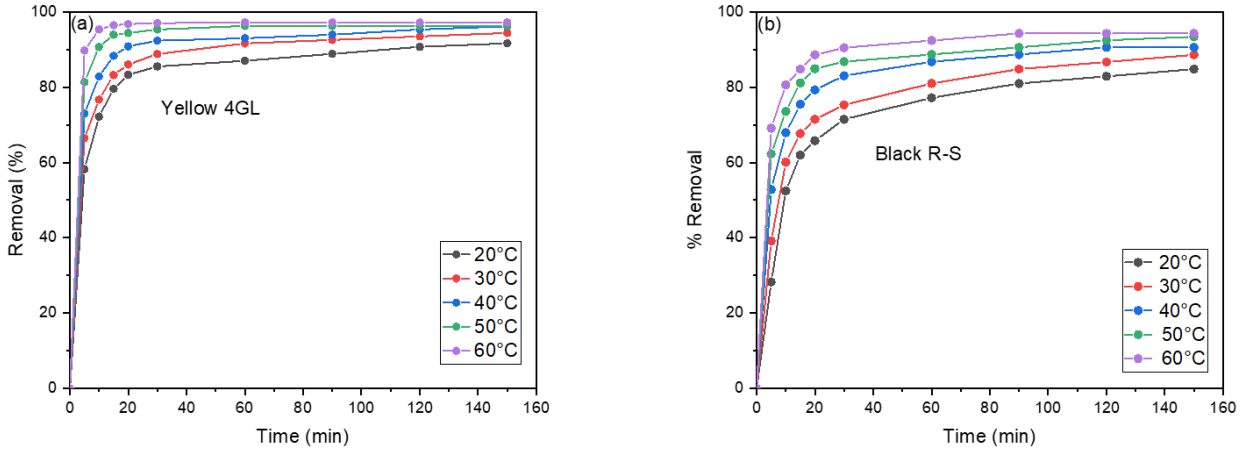

Figure 8. (a) Effect of Black R-S and (b) Yellow 4GL temperature on removal efficiency (0.03 g material, 50 mL of Yellow 4GL or Black R–S dye).

process using the PEI-magnetic bagasse composite. The data reveal two distinct linear regimes, designated as Stage 1 and Stage 2. During Stage 1, adsorption occurs rapidly, predominantly at the external surface and within larger pores near the surface. The steep slopes observed (16.56 for Yellow 4GL and 73.77 for Black R-S) are indicative of strong binding interactions facilitated by the amino-rich PEI layer and efficient boundary layer diffusion within the porous structure. High R^2 values (0.9967 for Yellow 4GL and 0.991 for Black R-S) confirm that this initial phase is well-described by the intra-particle diffusion model. In Stage 2, the slopes decrease substantially (2.05 for Yellow 4GL and 1.50 for Black R-S), reflecting slower adsorption kinetics controlled primarily by the diffusion of dye molecules into the deeper pores of the adsorbent. The fact that the linear plots do not pass through the origin suggests that intra-particle diffusion is not the sole rate-limiting step; additional factors, such as film diffusion, pore-size distribution, and specific dye–adsorbent interactions, also play significant roles in the overall adsorption mechanism [26].

3.5 Thermodynamics

Table 3 shows the thermodynamic parameters for the adsorption of Yellow 4GL and Black R-S dyes at different temperatures. The Gibbs free energy (ΔG°) of Yellow 4GL and Black R-S decreases with increasing temperature, from -33.22 kJ/mol at 293 K to -37.76 kJ/mol and -28.91 kJ/mol to -32.86 kJ/mol, respectively. This result suggests that adsorption processes occur spontaneously and become more favorable at higher temperatures. Both dyes had positive enthalpy change (ΔH°) values, with Yellow 4GL at 0.028 kJ/mol and Black R-S at 0.022 kJ/mol, indicating endothermic adsorption. Positive entropy changes (ΔS°) reported for both dyes (0.113 kJ/mol·K for Yellow 4GL and 0.099 kJ/mol·K for Black R-S) indicate increased

Table 2. Kinetic model parameters of pseudo-first-order and pseudo-second-order for Yellow 4GL and Black R-S.

Dye	C_0 (mg/L)	Pseudo-first order			Pseudo-second order		
		k_1(min^{-1})	q_e (mg/g)	R^2	k_2 (min^{-1})	q_e (mg/g)	R^2
Yellow 4GL	25	0.0187	4.98	0.870	0.0171	62.50	0.9999
	50	0.031	22.29	0.821	0.0396	121.95	1.0000
	75	0.033	53.39	0.955	0.0016	178.57	1.0000
	100	0.033	96.59	0.977	0.0008	232.55	0.9999
	125	0.020	96.31	0.937	0.0006	263.15	0.9999
	150	0.009	149.41	0.830	0.0004	227.27	0.9995
Black R – S	25	0.0200	4.79	0.820	0.1817	60.97	1.0000
	50	0.0289	19.90	0.886	0.0050	120.48	0.9999
	75	0.0122	36.01	0.817	0.0024	175.43	0.9999
	100	0.0257	55.57	0.9503	0.0015	227.27	0.9999
	125	0.0302	71.77	0.9540	0.0011	270.27	0.9999
	150	0.0067	103.39	0.5975	0.0010	227.27	0.9994

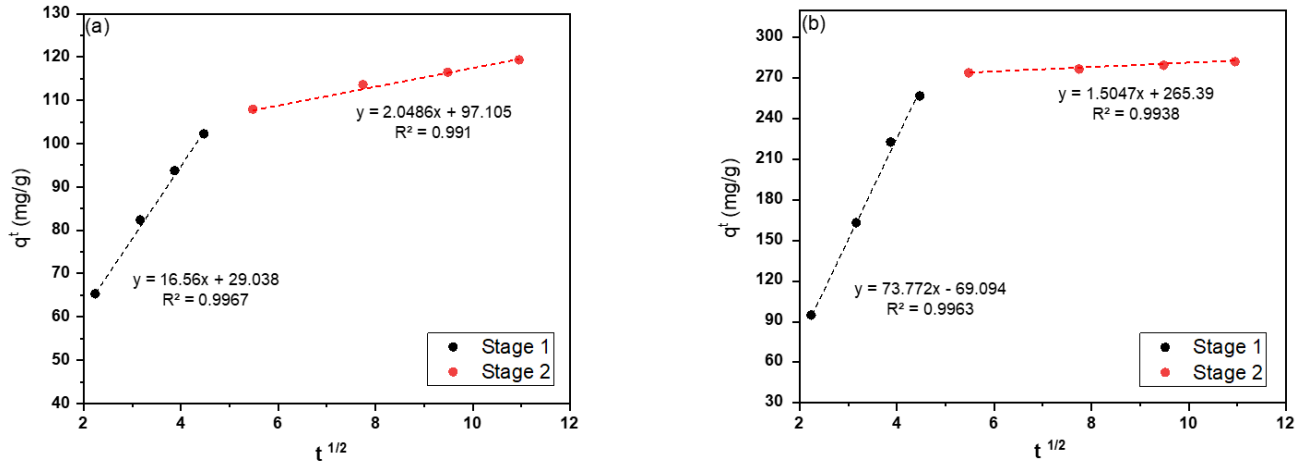

Figure 9. The intraparticle diffusion for the adsorption of (a) Yellow 4GL and (b) Black R-S

randomness at the solid-liquid interface during adsorption. The larger ΔH° for Yellow 4GL compared to Black R-S shows that adsorption of Yellow 4GL requires more energy, possibly due to changes in the molecular interactions between the dye molecules and the adsorbent surface.

3.6 Reusability and Regeneration Study

The regeneration ability of a PEI-magnetic bagasse composite was investigated over five successive adsorption-desorption cycles with Black R-S and Yellow 4GL dyes (Figure 10). In the first cycle, removal efficiencies for both dyes approached 95%, revealing the improved material's high adsorption capacity. Although performance gradually declined with each reuse, the adsorbent maintained around 85% removal efficiency by the fifth cycle. The remarkable regeneration efficiency and structural stability of PEI-magnetic bagasse contribute to its promise as a reusable and cost-effective adsorbent.

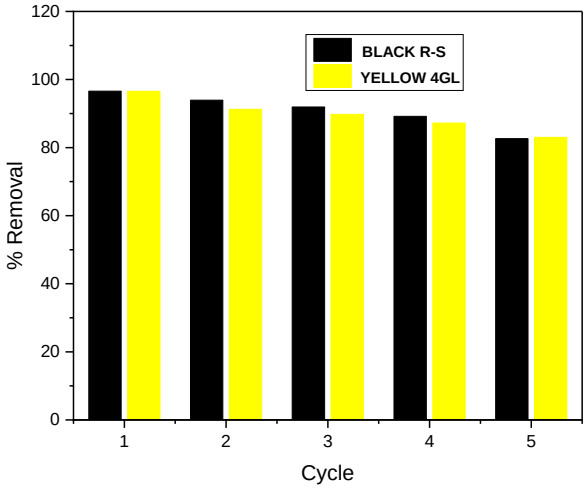

Figure 10. The reusability of PEI-magnetic bagasse composite.

4. Conclusions

This study successfully synthesized a magnetic polyethyleneimine (PEI)-modified bagasse composite by utilizing sugarcane bagasse, in conjunction with Fe_3O_4 nanoparticles and PEI. The composite demonstrated considerable potential for the removal of Yellow 4GL and Black R–S anionic dyes. Adsorption studies indicated that the process adheres to the Langmuir isotherm, achieving maximum adsorption capacities of 185.19 mg/g for Yellow 4GL and 204.08 mg/g for Black R–S. Moreover, the pseudo-second-order kinetic model provided the best fit for the experimental data with correlation coefficients (R^2 ~ 1.0000), suggesting that the adsorption mechanism is predominantly governed by chemisorption, with electrostatic attraction and hydrogen bonding playing key roles. The negative ΔG° values observed for both dyes confirm that the adsorption processes are spontaneous and become more favorable at high temperatures. The presence of PEI enhanced adsorption capacity by introducing functional amino groups, while the magnetic properties facilitated material recovery for reuse. The findings provide a scientific basis for scaling this material for practical applications in wastewater treatment, paving the way for sustainable solutions to removal dye pollution.

Conflict of interest

There are no conflicts to declare.

Data Availability

These data are available upon request.

Acknowledgement

The authors would like to thank the Industrial University of Ho Chi Minh City and Ho Chi Minh City University of Industry and Trade for facilities support.

Table 3. The thermodynamic variables at different temperatures.

Temperature (K)	Yellow 4GL		Black R - S			
	ΔG^0 (kJ/mol)	ΔS^0 (kJ/mol·K)	ΔH^0 (kJ/mol)	ΔG^0 (kJ/mol)	ΔS^0 (kJ/mol·K)	ΔH^0 (kJ/mol)
293	-33.22			-28.91		
303	-34.36			-29.91		
313	-35.49	0.113	0.028	-30.89	0.099	0.022
323	-36.62			-31.88		
333	-37.76			-32.86		

CRediT Author Statement

Author Contributions: Methodology and formal analysis (Thi Thuy Hong Vu); Data curation (Thi Diem Bui); Methodology (Nguyen Le Huu Khanh); Investigation, Writing - Review and Editing (Thi Hong Anh Nguyen). All authors have read and agreed to the published version of the manuscript.

References

[1] Baloo, L., Isa, M.H., Sapari, N. Bin, Jagaba, A.H., Wei, L.J., Yavari, S., Razali, R., Vasu, R. (2021). Adsorptive removal of methylene blue and acid orange 10 dyes from aqueous solutions using oil palm wastes-derived activated carbons. *Alexandria Engineering Journal*, 60(6), 5611–5629. DOI: 10.1016/j.aej.2021.04.044.

[2] Pavithra, K., Engineering, V.J.-J. of I. and, 2019, undefined (2019). Removal of colorants from wastewater: A review on sources and treatment strategies. *Journal of Industrial and Engineering Chemistry*, 75, 1–19. DOI: 10.1016/j.jiec.2019.02.011.

[3] Xiang, H., Min, X., Tang, C.-J., Sillanpää, M., Zhao, F. (2022). Recent advances in membrane filtration for heavy metal removal from wastewater: A mini review. *Journal of Water Process Engineering*, 49, 103023. DOI: 10.1016/j.jwpe.2022.103023.

[4] Bui Bao Long, P., Nguyen, V.C., Pham, H.A. Le, Ta, Q.T.H., Dang, H.P. (2025). Effect of the Dimethylformamide/Isopropanol Solvent Ratio on the Structure, Optical Properties, and Photodegradation Performance of RhB Using Bi-MOF. *Bulletin of Chemical Reaction Engineering & Catalysis*, 20(1), 166–176. DOI: 10.9767/bcrec.20345.

[5] Aruna, Bagotia, N., Sharma, A.K., Kumar, S. (2021). A review on modified sugarcane bagasse biosorbent for removal of dyes. *Chemosphere*, 268, 129309. DOI: 10.1016/j.chemosphere.2020.129309.

[6] Deng, Z., Luo, Y., Bian, M., Guo, X., Zhang, N. (2023). Synthesis of easily renewable and recoverable magnetic PEI-modified Fe3O4 nanoparticles and its application for adsorption and enrichment of tungsten from aqueous solutions. *Environmental Pollution*, 330, 121703. DOI: 10.1016/j.envpol.2023.121703.

[7] Xia, T., Guan, Y., Yang, M., Xiong, W., Wang, N., Zhao, S., Guo, C. (2014). Synthesis of polyethylenimine modified Fe3O4 nanoparticles with immobilized Cu2+ for highly efficient proteins adsorption. *Colloids and Surfaces A: Physicochemical and Engineering Aspects*, 443, 552–559. DOI: 10.1016/j.colsurfa.2013.12.026.

[8] Tsague, C.F., Abbo, H.S., Yufanyi, D.M., Ondoh, A.M., Titinchi, S.J.J. (2023). Recyclable functionalized polyethyleneimine-coated magnetic nanoparticles for efficient removal of lead from aqueous solutions. *Journal of Chemical Technology & Biotechnology*, 98(8), 2023–2038. DOI: 10.1002/jctb.7423.

[9] Chen, B., Xie, H., Zhang, A., Liu, N., Li, Q., Guo, J., Su, B. (2019). Synthesis of PEI-Functionalized Magnetic Nanoparticles for Capturing Bacteria. *Journal of Wuhan University of Technology-Mater Sci Ed*, 34(1), 236–242. DOI: 10.1007/s11595-019-2041-y.

[10] Liou, T.H., Huang, J.J. (2024). Efficient Removal of Hazardous P-Nitroaniline from Wastewater by Using Surface-Activated and Modified Multiwalled Carbon Nanotubes with Mesostructure. *Toxics*, 12(1) DOI: 10.3390/toxics12010088.

[11] Zulfiqar, N., Nadeem, R., Musaimi, O.A. (2023). Photocatalytic Degradation of Antibiotics via Exploitation of a Magnetic Nanocomposite: A Green Nanotechnology Approach toward Drug-Contaminated Wastewater Reclamation. *ACS Omega*. 9, 7, 7986–8004. DOI: 10.1021/acsomega.3c08116

[12] Yakut, Ş.M. (2023). Treatment of textile wastewater with cherry laurel leaves and waste potato peels. *Eurasian Journal of Science Engineering and Technology*, 4(1) DOI: 10.55696/ejset.1296953.

[13] Samarghandi, M.R., Zarrabi, M., Amrane, A., Soori, M.M., Sepehr, M.N. (2018). Removal of acid black dye by pumice stone as a low cost adsorbent: kinetic, thermodynamic and equilibrium studies. *Environmental Engineering and Management Journal*, 12(11) DOI: 10.30638/eemj.2013.265.

[14] Nguyen, V.C., Hieu, T.Q., Thien, P.T., Vu, L.D., V T, Le. (2017). Reusable starch-graft-polyaniline/Fe3O4 composite for removal of textile dyes. *Rasayan Journal of Chemistry*, 10(4), 1446–1454. DOI: 10.7324/RJC.2017.1041894.

[15] Hassan, M.M., Carr, C.M. (2021). Biomass-derived porous carbonaceous materials and their composites as adsorbents for cationic and anionic dyes: A review. *Chemosphere* 265, February 2021, 129087. DOI: 10.1016/j.chemosphere.2020.129087

[16] Ngamsurach, P., Nemkhuntod, S., Chanaphan, P., Praipipat, P. (2022). Modified Beaded Materials from Recycled Wastes of Bagasse and Bagasse Fly Ash with Iron(III) Oxide-Hydroxide and Zinc Oxide for the Removal of Reactive Blue 4 Dye in Aqueous Solution. *ACS Omega*, 7(39) DOI: 10.1021/acsomega.2c03250.

[17] Birniwa, A.H., Mahmud, H.N.M.E., Abdullahi, S.S., Habibu, S., Jagaba, A.H., Ibrahim, M.N.M., Ahmad, A., Alshammari, M.B., Parveen, T., Umar, K. (2022). Adsorption Behavior of Methylene Blue Cationic Dye in Aqueous Solution Using Polypyrrole-Polyethylenimine Nano-Adsorbent. *Polymers*, 14(16) DOI: 10.3390/polym14163362.

[18] Thi Hong Anh, N., Thanh Phuc, T., Nguyen Minh An, T., Pho Quoc, H., Nguyen, V.C. (2020). Microwave-Assisted Preparation of Magnetic Citric Acid-Sugarcane Bagasse for Removal of Textile Dyes. *Indonesian Journal of Chemistry*, 20(5), 1101. DOI: 10.22146/ijc.48713.

[19] Maryana, R., Muryanto, Triwahyuni, E., Oktaviani, O., Prasetia, H., Das, A.K., Sudiyani, Y. (2022). Extraction of Cellulose Acetate from Cajuput (Melaleuca leucadendron) Twigs and Sugarcane (Saccharum officinarum) Bagasse by Environmentally Friendly Approach. *Waste and Biomass Valorization*, 13(3), 1535–1545. DOI: 10.1007/s12649-021-01610-y.

[20] Huong, T.T., Doan Trang, T.Y. (2023). Synthesis of a cost-effective magnetic nanoparticles coated sugarcane bagasse and testing tetracycline removal capacity. In: *E3S Web of Conferences*. DOI: 10.1051/e3sconf/202344305005.

[21] Moretti, M.M. de S., Perrone, O.M., Nunes, C. da C.C., Taboga, S., Boscolo, M., da Silva, R., Gomes, E. (2016). Effect of pretreatment and enzymatic hydrolysis on the physical-chemical composition and morphologic structure of sugarcane bagasse and sugarcane straw. *Bioresource Technology*, 219, 773–777. DOI: 10.1016/j.biortech.2016.08.075.

[22] Dermawan, D., Satriavi, A.D., Nurhidayati, D.I., Firnandi, R., Mayangsari, N.E., Ramadani, T.A., Widiana, D.R., Juniani, A.I., Mujiyanti, D.R., Wang, Y.F. (2025). Composite adsorbent from sugarcane (Saccharum officinarum) bagasse biochar generated from atmospheric pressure microwave plasma pyrolysis process and nano zero valent iron (nZVI) for rapid and highly efficient Cr(VI) adsorption. *Case Studies in Chemical and Environmental Engineering*, 11, 101123. DOI: 10.1016/j.cscee.2025.101123.

[23] Abu Elgoud, E.M., Abd-Elhamid, A.I., Aly, H.F. (2024). Adsorption behavior of Mo(VI) from aqueous solutions using tungstate-modified magnetic nanoparticle. *Environmental Science and Pollution Research*, 31(12), 18900–18915. DOI: 10.1007/s11356-024-32251-y.

[24] Congsomjit, D., Areeprasert, C. (2021). Hydrochar-derived activated carbon from sugar cane bagasse employing hydrothermal carbonization and steam activation for syrup decolorization. *Biomass Conversion and Biorefinery*, 11(6), 2569–2584. DOI: 10.1007/s13399-020-00635-y.

[25] Aramesh, N., Bagheri, A.R., Bilal, M. (2021). Chitosan-based hybrid materials for adsorptive removal of dyes and underlying interaction mechanisms. *International Journal of Biological Macromolecules*, 183, 399–422. DOI: 10.1016/j.ijbiomac.2021.04.158.

[26] Nizam, N.U.M., Hanafiah, M.M., Mahmoudi, E., Halim, A.A., Mohammad, A.W. (2021). The removal of anionic and cationic dyes from an aqueous solution using biomass-based activated carbon. *Scientific Reports*, 11(1), 8623. DOI: 10.1038/s41598-021-88084-z.

[27] Nguyen, T.H.A., Tran, T.D.M., Ky Vo, T., Nguyen, Q.T., Nguyen, V.-C. (2023). Facile synthesis of low-cost chitosan/Fe3O4@C composite for highly efficient adsorption of levofloxacin antibiotic. *Chemical Engineering Communications*, 210(7), 1073–1085. DOI: 10.1080/00986445.2022.2053680.

[28] Al-Ghouti, M.A., Al-Absi, R.S. (2020). Mechanistic understanding of the adsorption and thermodynamic aspects of cationic methylene blue dye onto cellulosic olive stones biomass from wastewater. *Scientific Reports*, 10(1), 15928. DOI: 10.1038/s41598-020-72996-3.

[29] Kapoor, R.T., Rafatullah, M., Siddiqui, M.R., Khan, M.A., Sillanpää, M. (2022). Removal of Reactive Black 5 Dye by Banana Peel Biochar and Evaluation of Its Phytotoxicity on Tomato. *Sustainability*, 14(7) DOI: 10.3390/su14074176.

[30] Hasani, N., Selimi, T., Mele, A., Thaçi, V., Halili, J., Berisha, A., Sadiku, M. (2022). Theoretical, Equilibrium, Kinetics and Thermodynamic Investigations of Methylene Blue Adsorption onto Lignite Coal. *Molecules*, 27(6), 1856. DOI: 10.3390/molecules27061856.